

# Dynamics near the central singularity in spherical collapse

Jun-Qi Guo<sup>1,\*</sup>

<sup>1</sup>*School of Physics and Technology, University of Jinan, Jinan 250022, Shandong, China*

(Dated: 8th July 2022)

We study the dynamics near the central singularity in spherically symmetric collapse of a massless scalar field toward Schwarzschild black hole formation. The equations of motion take different simplified forms in the early and late stages of the singularity curve, enabling us to extract some fine structures and universal features for the metric and scalar field along the singularity curve. The numerical results show that the spacetime near the central singularity asymptotes to the Schwarzschild limit in the late stage of collapse, verifying the no-hair theorem inside black holes.

## I. INTRODUCTION

Rich, nonlinear dynamics exists in curved, empty spacetime. Achievements have been made in related branches, e.g., gravitational collapse, spacetime singularities and gravitational waves etc [1–16].

In this paper, we study the dynamics near the central singularity in spherical scalar collapse toward Schwarzschild black hole formation. Analytic information is crucial for understanding the nature of collapse and spacetime singularities. However, due to the complexity of the Einstein equations, analytic information is usually unavailable and numerical simulations are implemented, instead. The good thing is that, gravity near singularities is extremely strong, such that in some circumstances the equations of motion take simplified forms and approximate analytic information on the metric and matter can be extracted. Treating the scalar field as a linear perturbation and neglecting the backreaction of the scalar field on the geometry, Doroshkevich and Novikov studied the dynamics near the central singularity in a Schwarzschild black hole, and found that the scalar field diverges logarithmically with the areal radius  $r$  [17]. A full asymptotic expansion solution to the wave equation near the singularity was obtained by Fournodavlos and Sbierski [18]. Taking into account the backreaction of the scalar field on the geometry and using the simplified assumption of quasi homogeneity of spacetime, Burko obtained a series-expansion solution for the metric and scalar field near the central singularity in spherical scalar collapse [19, 20]. The blow-up rates for the Kretschmann scalar were investigated in Refs. [21–23]. For spherical scalar collapse, via numerical simulation and asymptotic analysis, approximate analytic solutions for the spacetime, scalar field and Kretschmann scalar near the central singularity were obtained in Refs. [24, 25]. Compared to Ref. [24], in this paper, with improved code and further analysis, we obtain more detailed analytic information in both the early and late stages of the singularity curve, and find that the metric and scalar field display some universal features.

The paper is organized as below. The methodology for simulating spherical scalar collapse is depicted in Sec. II. We explore the dynamics near the singularity in the late and early stages of collapse in Secs. III and IV, respectively. The no-hair theorem inside black holes is studied in Sec. V. The results are summarized in Sec. VI. Throughout the paper, we set  $G = c = 1$ .

## II. METHODOLOGY

Collapse of a massless scalar field  $\phi$  in spherical symmetry is simulated in the coordinates [26],

$$ds^2 = e^{-2\sigma(t,x)}(-dt^2 + dx^2) + r^2(t,x)d\Omega^2. \quad (1)$$

The energy-momentum tensor for  $\phi$  is  $T_{\mu\nu} = \phi_{,\mu}\phi_{,\nu} - (1/2)g_{\mu\nu}g^{\alpha\beta}\phi_{,\alpha}\phi_{,\beta}$ . Then the equations of motion read

$$r(-r_{,tt} + r_{,xx}) - r_{,t}^2 + r_{,x}^2 = e^{-2\sigma}, \quad (2)$$

$$-\sigma_{,tt} + \sigma_{,xx} + \frac{r_{,tt} - r_{,xx}}{r} + 4\pi(\phi_{,t}^2 - \phi_{,x}^2) = 0, \quad (3)$$

$$-\phi_{,tt} + \phi_{,xx} + \frac{2}{r}(-r_{,t}\phi_{,t} + r_{,x}\phi_{,x}) = 0. \quad (4)$$

For numerical stability concern near the center,  $\eta(\equiv r^2)$  [26] and the Misner-Sharp mass  $m$  [27],  $g^{\mu\nu}r_{,\mu}r_{,\nu} \equiv 1 - 2m/r$ , are used as auxiliary variables. Then Eqs. (2) and (3) can be rewritten as

$$-\eta_{,tt} + \eta_{,xx} = 2e^{-2\sigma}, \quad (5)$$

$$-\sigma_{,tt} + \sigma_{,xx} - e^{-2\sigma} \cdot \frac{2m}{r^3} + 4\pi(\phi_{,t}^2 - \phi_{,x}^2) = 0. \quad (6)$$

The dynamics of  $m$  is described by

$$m_{,t} = 4\pi r^2 \cdot e^{2\sigma} \left[ -\frac{1}{2}r_{,t}(\phi_{,t}^2 + \phi_{,x}^2) + r_{,x}\phi_{,t}\phi_{,x} \right]. \quad (7)$$

In the simulation, we use finite-difference method and leap-frog scheme. The numerical setup is basically the same as that in Ref. [28], and the code is second-order convergent. The initial value for the scalar field is  $\phi(t=0, x) = a \tanh(x - x_0)$  with  $a = 0.1$  and  $x_0 = 5$ . Mesh refinement [24, 29] is implemented in studying the dynamics near the singularity.

\*Electronic address: sps.guojq@ujn.edu.cn

### III. RESULT I: DYNAMICS IN THE LATE STAGE WITH $|C| < \sqrt{1/2}$

The numerical results show that the dynamics is different at small and large  $x$  along the singularity curve. Correspondingly, we separate the singularity curve into early (small  $x$ ) and late (large  $x$ ) stages. In the early (late) stage, the quantity  $|C|$  in Eq. (14) is less (greater) than  $\sqrt{1/2}$ , and the metric quantity  $\sigma$  asymptotes to  $+\infty$  ( $-\infty$ ) [see Figs. 1(a), 1(h) and 1(j) and Eqs. (13), (15) and (19)]. We analyze the dynamics in the late and early stages in this and next sections, respectively.

#### A. Dynamics in the late stage with $|C| < \sqrt{1/2}$

The numerical results for the apparent horizon and singularity curve  $r = 0$  of the black hole forming in collapse are plotted in Fig. 1(a). It can be shown that near the central singularity of a Schwarzschild black hole, the ratios between the spatial and temporal derivatives for  $r$  and  $\eta(=r^2)$  are expressed in terms of the slope  $J$  of the singularity curve (see the Appendix). It was also found that in spherical scalar collapse toward black hole formation, near the central singularity, this relation is also true for the quantities of  $r$ ,  $\sigma$  and  $\phi$  [24]. In this paper, with more accurate code, we find that such a relation also holds for  $\eta$  in the late stage of singularity formation in scalar collapse for which  $|C| > \sqrt{1/2}$  [see Figs. 2(b) and 2(c)]. In summary, we have

$$\begin{aligned} J^2 &\approx \left(\frac{r_{,x}}{r_{,t}}\right)^2 \approx \left(\frac{\eta_{,x}}{\eta_{,t}}\right)^2 \approx \left(\frac{\sigma_{,x}}{\sigma_{,t}}\right)^2 \approx \left(\frac{\phi_{,x}}{\phi_{,t}}\right)^2 \\ &\approx \frac{r_{,xx}}{r_{,tt}} \approx \frac{\eta_{,xx}}{\eta_{,tt}} \approx \frac{\sigma_{,xx}}{\sigma_{,tt}} \approx \frac{\phi_{,xx}}{\phi_{,tt}}. \end{aligned} \quad (8)$$

With Eq. (8), Eqs. (3)-(5) can be reduced to

$$-\sigma_{,tt} + \frac{r_{,tt}}{r} \approx -4\pi\phi_{,t}^2, \quad (9)$$

$$\phi_{,tt} \approx -\frac{2r_{,t}\phi_{,t}}{r}, \quad (10)$$

$$(-1 + J^2)\eta_{,tt} \approx 2e^{-2\sigma}. \quad (11)$$

The quantities  $r$ ,  $\sigma$  and  $\phi$  can be well approximated by the following expressions [24],

$$r \approx A\xi^\beta, \quad (12)$$

$$\sigma \approx B \ln \xi + \sigma_0, \quad (13)$$

$$\sqrt{8\pi}\phi \approx C \ln \xi + \phi_0, \quad (14)$$

where  $\xi = t_0 - t$  and  $t_0$  is the coordinate time on the singularity curve. We respectively fit the numerical results

of  $r$ ,  $\sigma$  and  $\phi$  according to Eqs. (12)-(14) with the fitting results being shown in Fig. 1. Substitution of Eqs. (12)-(14) into (9) yields [24]

$$B \approx \beta(1 - \beta) - \frac{1}{2}C^2. \quad (15)$$

As shown in Fig. 2(a), near the singularity,  $-rr_{,tt} \approx r_{,t}^2$ , which implies that  $\beta \approx 1/2$ . Considering this result and substituting Eqs. (12), (13) and (15) into (11), we arrive at the first line of Eq. (16). As will be discussed in Sec. V, the mass of the black hole forming in the late stage of collapse is approximately expressed by Eq. (33). Combining this equation and the first line of (16), we obtain the second line of (16),

$$\begin{aligned} \beta &\approx \frac{1}{2} \left[ 1 - \frac{2}{A^2(1 - J^2)e^{2\sigma_0}} \xi^{\frac{1}{2} + C^2} \right] \\ &\approx \frac{1}{2} \left( 1 - \frac{A}{4m_0} \xi^{\frac{1}{2} + C^2} \right). \end{aligned} \quad (16)$$

$m_0$  is the eventual mass of the black hole forming in collapse. In the circumstances where  $x \gg 1$  along the singularity curve and  $\xi \rightarrow 0$ , there are  $|C| \rightarrow 0$  and  $\beta \rightarrow 1/2$ . Then with Eq. (12), the second line of (16) becomes

$$\beta \approx \frac{1}{2} \left( 1 - \frac{r}{4m_0} \right). \quad (17)$$

Note that the factor  $2/[A^2(1 - J^2)e^{2\sigma_0}]$  in the first line of (16) was omitted in Ref. [24].

We obtain  $\beta$  by fitting the numerical results of  $r$  vs.  $\xi$  according to Eq. (12) for a certain range of  $\xi$ ,  $[\Delta\xi, \sim 180\Delta\xi]$ , where  $\Delta\xi$  is the grid distance. On the other hand, we also obtain  $\beta$  from the first line of Eq. (16) with  $\xi = 122\Delta\xi$ . As shown in Fig. 1(f), the results for  $\beta$  by these two approaches match well.

#### B. Discussions

Figure 1(f) seems to show that  $\beta$  keeps decreasing as  $x$  increases. However, a much-less-than-one-half  $\beta$  would be very different from the Schwarzschild limit (which is  $1/2$ ). Actually, in Fig. 1(f),  $\Delta\xi$  is roughly constant for  $2 \leq x \leq 4$ . For even larger  $x$ ,  $\Delta\xi$  needs to be further smaller, such that the region where  $\xi \sim \Delta\xi$  on the slice of  $x = \text{Constant}$  remains inside the horizon and in the vicinity of the singularity. Consequently, near the singularity,  $\beta$  will remain close to  $1/2$  for large  $x$  as expected.

Here we briefly interpret Eq. (8). Consider a group of contour lines of  $r$  and  $\eta(=r^2)$  near the singularity curve in a very local region shown in Fig. 3. From Fig. 3, one can straightforwardly obtain  $J \approx |r_{,x}/r_{,t}| \approx |\eta_{,x}/\eta_{,t}|$  and  $J^2 \approx |r_{,xx}/r_{,tt}| \approx |\eta_{,xx}/\eta_{,tt}|$ . Note that, the values of  $\sigma$  and  $\phi$  described by Eqs. (13) and (14) are determined by  $\ln \xi$  with  $\xi \equiv t_0 - t$  and the coefficients  $B$  and  $C$ . Near the singularity, compared to  $\ln \xi$ , the coefficients  $B$  and

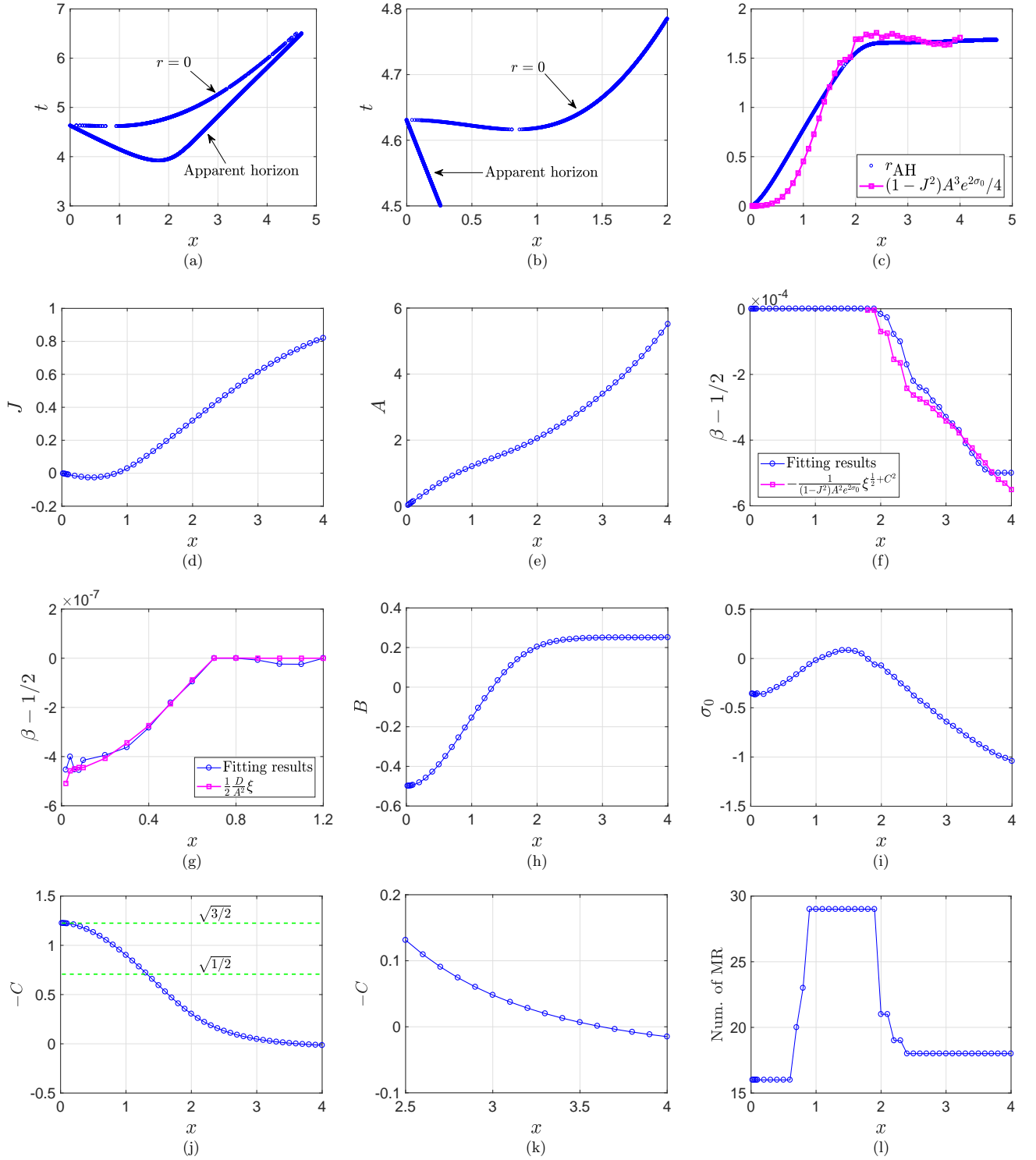


Figure 1: (color online). Numerical results for spherical scalar collapse toward Schwarzschild black hole formation. (a) and (b): Apparent horizon and singularity curve. (c) Radius of the apparent horizon. (d) Slope of the singularity curve,  $J$ .  $|J|$  is obtained from the numerical results of  $|r_{,x}/r_{,t}|$ . The sign of  $J$  is obtained by checking the shape of the singularity curve. (e)-(g): The fitting results for  $A$  and  $\beta$  in Eq. (12),  $r \approx A\xi^\beta$ . (h) and (i): The fitting results for  $B$  and  $\sigma_0$  in Eq. (13),  $\sigma \approx B \ln \xi + \sigma_0$ . (j) and (k): The fitting results for  $C$  in Eq. (14),  $\sqrt{8\pi}\phi \approx C \ln \xi + \phi_0$ . (l) Numbers of mesh refinements near the singularity curve, which are also approximately the minimal numbers of mesh refinements needed to make Eqs. (8) or (18) valid in the simulation. For each round of mesh refinement, we insert one new data point between every two neighbouring grid points in both spatial and temporal directions via interpolation.

$C$  change more slowly [see Figs. 1(h) and 1(j)]. Then at least in a very local region of the contour lines of  $r$ ,  $\sigma$

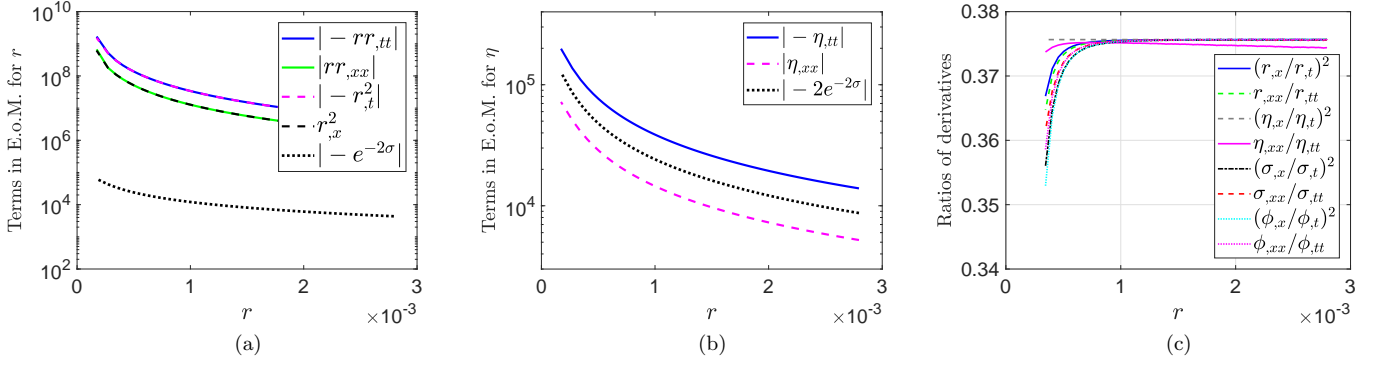


Figure 2: (color online). Numerical results on the late-stage dynamics near the central singularity on the slice of  $x = 3$ . (a) Terms in Eq. (2),  $r(-r_{,tt} + r_{,xx}) - r_{,t}^2 + r_{,x}^2 = e^{-2\sigma}$ . Near the singularity,  $-rr_{,tt} \approx r_{,t}^2$ , which yields  $r \approx A\xi^{1/2}$ . (b) Terms in Eq. (5),  $-\eta_{,tt} + \eta_{,xx} = 2e^{-2\sigma}$ . Near the singularity, the equation is reduced to (11):  $(-1 + J^2)\eta_{,tt} = 2e^{-2\sigma}$ . (c) Ratios between spatial and temporal derivatives for  $r$ ,  $\eta(=r^2)$ ,  $\sigma$  and  $\phi$ . The ratios are all approximately equal to  $J^2$  ( $\approx 0.375$ ). Note that on the slice of  $x = 3$ , the slope of the singularity curve is  $J \approx 0.614$ .

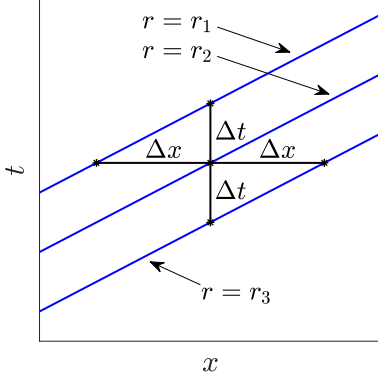


Figure 3: Pictorial illustration of the contour lines of  $r$  near the central singularity in a very local region. Denote  $J$  as the slope of the contour lines.  $J \approx \Delta t / \Delta x \approx r_{,x} / r_{,t}$ , and  $J^2 \approx (\Delta t / \Delta x)^2 \approx r_{,xx} / r_{,tt}$ .

and  $\phi$  also take constant values. So the ratio results of (8) are also valid for  $\sigma$  and  $\phi$ .

#### IV. RESULT II: DYNAMICS IN THE EARLY STAGE WITH $|C| > \sqrt{1/2}$

##### A. Dynamics in the early stage with $|C| > \sqrt{1/2}$

As shown in Fig. 4(c), in the early stage of singularity formation, Eq. (8) remains valid, except for the term of  $\eta_{,xx}/\eta_{,tt}$ . So Eqs. (9), (10) and (12)-(15) still hold. Therefore, with Eqs. (13) and (15), one obtains that along the singularity curve, for small  $x$  where  $|C| > \sqrt{1/2}$ ,  $B$  is negative, and  $e^{-2\sigma}$  asymptotes to zero [see Fig. 4(b)]. Figure 4(b) also shows that in this case, near the singularity, Eq. (5) is simplified as

$$\eta_{,tt} \approx \eta_{,xx} \approx \text{Constant}. \quad (18)$$

As shown in Fig. 4(a), in this case, near the singularity, there is also  $-rr_{,tt} \approx r_{,t}^2$ , which implies that  $\beta \approx 1/2$ . Combining this result and Eqs. (12) and (18), we obtain

$$\beta \approx \frac{1}{2} \left( 1 + \frac{D}{A^2} \xi \right), \quad (19)$$

where  $D = \eta_{,tt} \approx \text{Constant}$  on the slice of  $x = \text{Constant}$ . The fitting results for  $\beta$  according to (12) and the analytic one by (19) match well [see Fig. 1(g)]. The values of  $\eta_{,tt}$  are shown in Fig. 5.

##### B. Dynamics near $x = r = 0$

In critical collapse of a spherically symmetric scalar field, the spacetime near the center before singularity formation is nearly conformally flat [28],

$$e^{-\sigma} \approx r_{,x} \approx \frac{r}{x}. \quad (20)$$

This is also true for collapse toward black hole formation (see Fig. 6). We interpret Eq. (20) as below:

(i) We set  $r = m \equiv 0$  at  $x = 0$ , which is sensible. With the definition of mass,  $g^{\mu\nu} r_{, \mu} r_{, \nu} \equiv 1 - 2m/r$ , Eq. (2) can be rewritten as

$$-r_{,tt} + r_{,xx} - e^{-2\sigma} \cdot \frac{2m}{r^2} = 0. \quad (21)$$

The quantity  $m_{,x}$  is

$$m_{,x} = 4\pi r^2 \cdot e^{2\sigma} \left[ \frac{1}{2} r_{,x} (\phi_{,t}^2 + \phi_{,x}^2) - r_{,t} \phi_{,t} \phi_{,x} \right]. \quad (22)$$

Noting that  $\phi_{,x} = 0$  at  $x = r = 0$ . So near  $x = r = 0$ ,  $m \propto r^3$ ,  $m/r = 0$ , and  $m/r^2 = 0$ . Considering  $r_{,t} = m/r \equiv 0$  at  $x = r = 0$  and  $g^{\mu\nu} r_{, \mu} r_{, \nu} \equiv 1 - 2m/r$ , we obtain  $e^{-\sigma} \approx r_{,x}$  near  $x = r = 0$ .

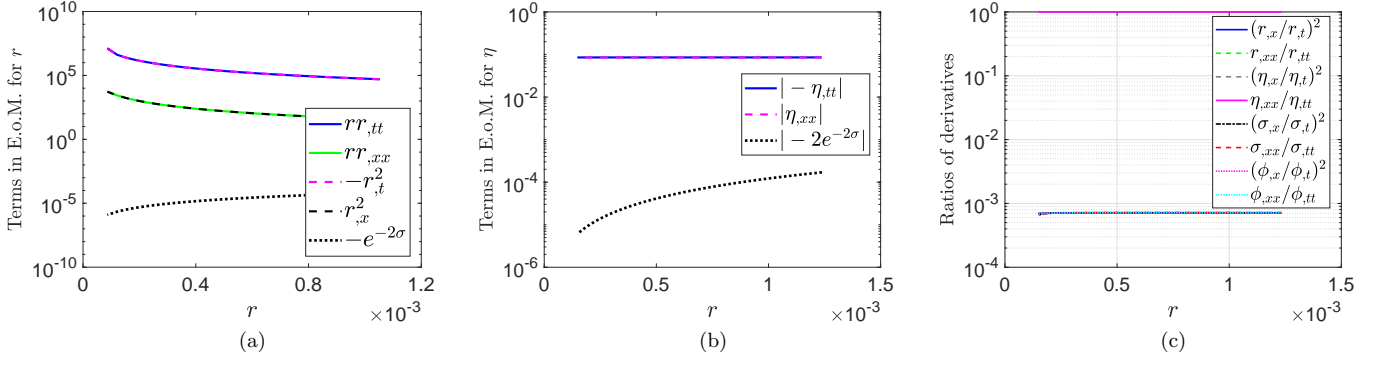


Figure 4: (color online). Numerical results on the early-stage dynamics near the central singularity on the slice of  $x = 0.5$ . (a) Terms in Eq. (2),  $r(-r_{,tt} + r_{,xx}) - r_{,t}^2 + r_{,x}^2 = e^{-2\sigma}$ . Near the singularity,  $-rr_{,tt} \approx r_{,t}^2$ , which yields  $r \approx A\xi^{1/2}$ . (b) Terms in Eq. (5),  $-\eta_{,tt} + \eta_{,xx} = 2e^{-2\sigma}$ . Near the singularity, the equation is reduced to (18):  $\eta_{,tt} \approx \eta_{,xx} \approx \text{Constant}$ . (c) Ratios between the spatial and temporal derivatives for  $r$ ,  $\eta(=r^2)$ ,  $\sigma$  and  $\phi$ .  $\eta_{,xx}/\eta_{,tt} \approx 1$ , and all other ratios are approximately equal to  $J^2$ .

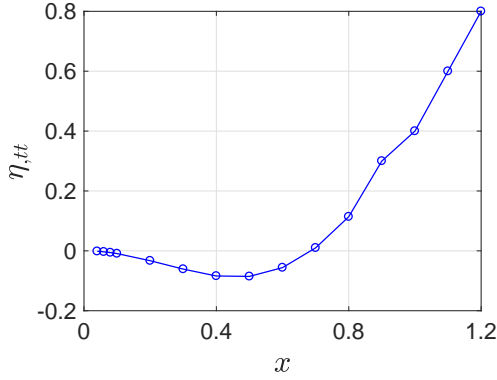


Figure 5:  $\eta_{,tt}$  in the early stage of singularity formation.

(ii) Combining Eq. (21) and the result of  $r_{,tt} = m/r^2 = 0$  at  $x = r = 0$ , one arrives at  $r_{,xx} \equiv 0$ , which implies that  $r \propto x$  near  $x = r = 0$ . Then we have  $r_{,x} \approx r/x$ . So Eq. (20) holds.

When the center just transits into singularity, the spacetime near the center is also conformally flat. In the vicinity of the singularity, the metric is expressed by the Kasner solution [24],

$$ds^2 = -d\tau^2 + \sum_{i=1}^3 \tau^{2p_i} dx_i^2. \quad (23)$$

$p_1 = (-1 + 2C^2)/(3 + 2C^2)$ , and  $p_2 = p_3 = 2/(3 + 2C^2)$ .  $q = 4C/(3 + 2C^2)$  describes the scalar field's contribution,  $\sqrt{8\pi}\phi = q \ln \tau$ . The Kasner exponents satisfy  $p_1 + p_2 + p_3 = 1$  and  $p_1^2 + p_2^2 + p_3^2 = 1 - q^2$ . For the conformally flat spacetime, there should be  $p_1 = p_2 = p_3 = 1/3$  and  $|C| \approx \sqrt{3/2}$ , which is well supported by Fig. 1(j).

Combining Eq. (12) and  $r \propto x$ , there are

$$A(x)|_{x \rightarrow 0} \approx kx \rightarrow 0, \quad r \approx kx\xi^\beta, \quad (24)$$

where  $k$  is a constant. The first part of Eq. (24) is verified by Fig. 1(e). Combination of Eqs. (8) and the second part

of (24) yields

$$J|_{x \rightarrow 0} \approx \left| \frac{r_{,x}}{r_{,t}} \right|_{x \rightarrow 0} \approx \frac{2\xi}{x}. \quad (25)$$

So near  $x = r = 0$ , the slope  $J$  asymptotes to zero, which is confirmed by Figs. 1(b) and 1(d).

Combining Eqs. (13), (15), (20) and (24), we have

$$k \approx e^{-\sigma_0}. \quad (26)$$

Equation (26) is verified by the numerical results:  $k \approx 1.45$  and  $e^{-\sigma_0} \approx 1.43$ .

### C. Discussions

We interpret/discuss the results obtained in this and the previous sections as below:

(i) In spherical scalar collapse, there is a competition between the kinetic energy of the scalar field and its gravitational potential energy. The former tends to disperse the mass-energy of the scalar field to infinity, while the latter tries to trap part of the energy inside a black hole [30]. For regularity concern in Eq. (4), we set  $\phi_{,x} \equiv 0$  at  $x = r = 0$ . So under this constraint,  $\phi$  is 'free' to move. Upon singularity formation, the quantity  $|C|$  is pushed to its maximum value  $\sqrt{3/2}$  by gravity. In this case, the ratios between the three terms in Eq. (9) are  $\sigma_{,tt} : -r_{,tt}/r : 4\pi\phi_{,t}^2 \approx 2 : 1 : 3$ . So the term for the kinetic energy of the scalar field,  $4\pi\phi_{,t}^2$ , dominates over the gravitational term,  $-r_{,tt}/r$ , and pushes  $\sigma$  to  $+\infty$ .

(ii) Although we think that the numerical results by Eq. (18) and (19) should be closely related to the boundary conditions at  $x = 0$ , we currently have no complete, intuitive interpretations on them.

(iii) When the singularity has formed, gravity gradually takes over the dominant role, the scalar field is directly

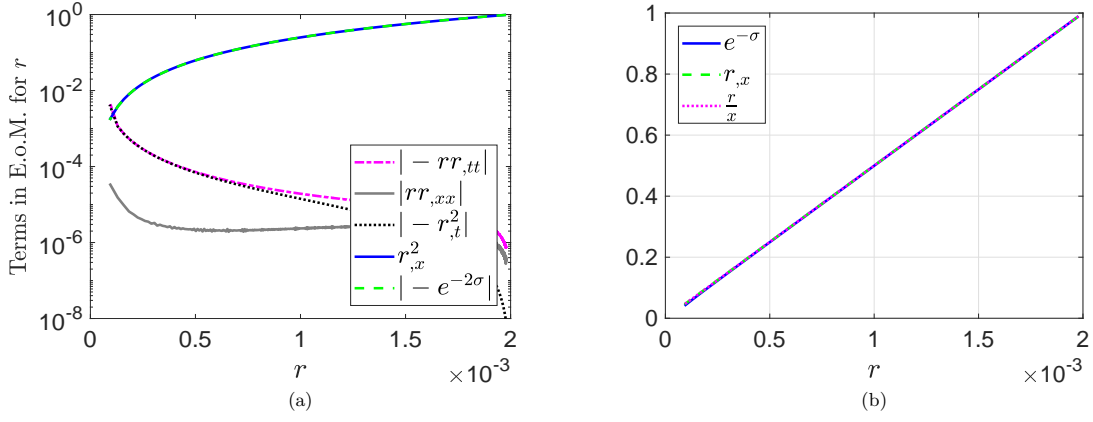


Figure 6: (color online). Conformal flatness of the spacetime near the center in spherical scalar collapse. The results are for the slice of  $x = 0.002$ . (a) Terms in Eq. (2),  $r(-r_{,tt} + r_{,xx}) - r_{,t}^2 + r_{,x}^2 = e^{-2\sigma}$ . Near the center,  $r_{,x} \approx e^{-\sigma}$ . (b)  $e^{-\sigma} \approx r_{,x} \approx r/x$ .

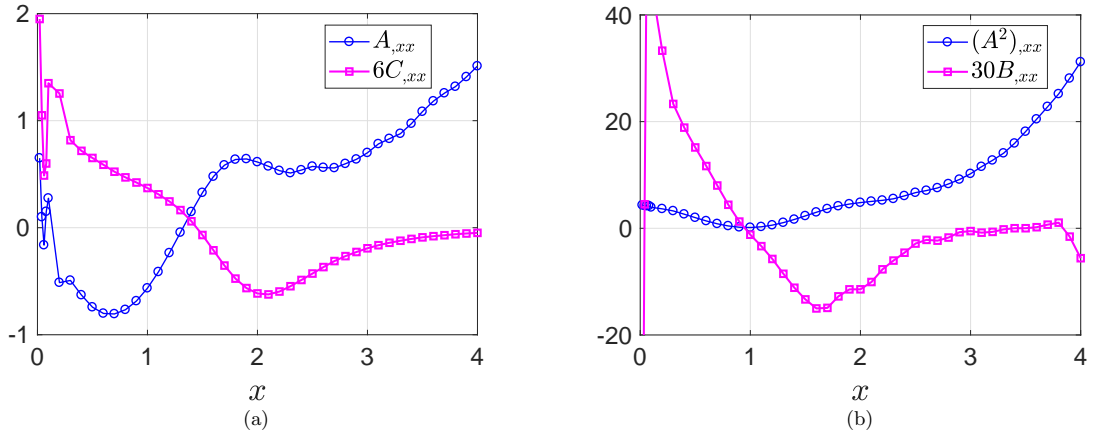


Figure 7: (color online). Some features on the quantities of  $A$  in Eq. (12),  $B$  in Eq. (13) and  $C$  in Eq. (14) along the singularity curve. (a)  $A_{,xx}$  vs.  $x$  and  $6C_{,xx}$  vs.  $x$ . (b)  $(A^2)_{,xx}$  vs.  $x$  and  $30B_{,xx}$  vs.  $x$ .

absorbed into the singularity without reflection at the center, and we obtain the results (11) and (16). Eventually, the quantity  $|C|$  asymptotes to zero.

(iv) In this paper, we obtain the fitting results for the parameters related to the metric functions and scalar field,  $A$ ,  $B$  and  $C$  along the singularity curve (see Fig. 1). These results have the same shapes as those obtained in Ref. [24], in which different initial data were used (see Figs. 6 and 11 in Ref. [24]). Therefore, we find universal features on the dynamics near the central singularity in spherical scalar collapse toward black hole formation.

(v) Analytic expressions for  $\{A, B, C\}$  vs.  $x$  are currently unavailable, and it may be meaningful to study this issue in the future.

Here we point out/summarize some features at certain points on the singularity curve:

(i)  $x = 0$ :  $A = A_{,xx} = J = 0$  [see Figs. 1(b), 1(d), 1(e) and 7(a)].

(ii)  $x \approx 0.84$ :  $(A^2)_{,xx} \approx B_{,xx} \approx J \approx 0$  [see Figs. 1(b), 1(d), 1(h) and 7(b)].

(iii)  $x \approx 1.32$ :  $|C| = \sqrt{1/2}$ ,  $A_{,xx} \approx C_{,xx} \approx 0$  [see Figs. 1(e), 1(j) and 7(a)]. At the place where  $x$  is slightly greater than 1.32,  $J \ll 1$ , then the terms of  $\eta_{,tt}$  and  $2e^{-2\sigma}$  in Eq. (5) are dominant,  $-\eta_{,tt} \approx 2e^{-2\sigma}$ . In the early stage where  $x < 1.32$ , the terms of  $\eta_{,tt}$  and  $\eta_{,xx}$  in Eq. (5) are dominant,  $\eta_{,tt} \approx \eta_{,xx}$ . At  $x \approx 1.32$ ,  $\eta_{,xx}$  and  $2e^{-2\sigma}$  are dominant,  $\eta_{,xx} \approx 2e^{-2\sigma}$  [see Fig. 8(b)].

(iv)  $x \rightarrow \infty$ : the Schwarzschild limit.

## V. RESULT III: ON THE NO-HAIR THEOREM INSIDE BLACK HOLES

### A. Background

Considering that, in the vicinity of a spacelike singularity, temporal derivatives are much higher than spatial

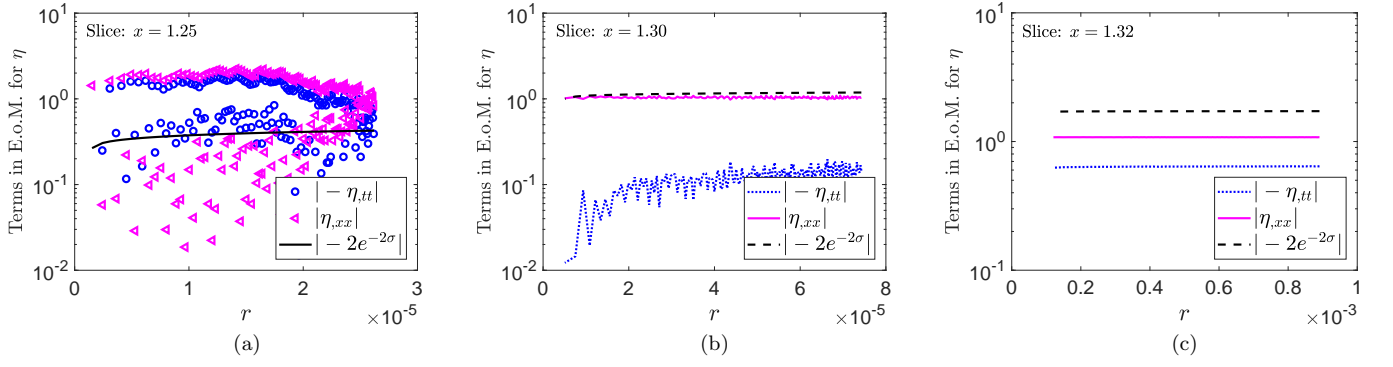


Figure 8: (color online). Behaviors of the terms in Eq. (5):  $-\eta_{,tt} + \eta_{,xx} = 2e^{-2\sigma}$ . (a) On the slice of  $x = 1.25$ ,  $\eta_{,tt} \approx \eta_{,xx}$ . (b) On the slice of  $x = 1.30$ ,  $\eta_{,xx} \approx 2e^{-2\sigma}$ . (c) On the slice of  $x = 1.32$ , the term of  $\eta_{,tt}$  contributes as a minor term.

ones, a simplifying assumption of homogeneity was used and a series-expansion solution for the metric functions and scalar field near the central singularity was obtained by Burko [19, 20]. The solutions in the first-order approximation were rewritten by Hansen *et al.* as below [31]:

$$ds^2 = f(r)dr^2 + h(r)dt^2 + r^2(t, x)d\Omega^2, \quad (27)$$

$$f(r) = -(\gamma + 2)\frac{1}{2m_0}r^{\beta+2}, \quad (28)$$

$$h(r) = 2m_0Cr^\gamma, \quad (29)$$

$$\sqrt{8\pi}\phi = \sqrt{2(\gamma + 1)}\ln r, \quad (30)$$

where  $m_0$  is the final black hole mass.

Spherical scalar collapse toward black hole formation was also simulated in the double-null coordinates by Burko. It was found that, along the singularity,  $\gamma$  has a local minimum of  $-1$ , and the temporal gradient of  $\gamma$  is zero at the local minima. So it was expected that, at these local minima, at least at the leading order, the singularity is Schwarzschild-like [19, 20].

## B. Results

(i) The Schwarzschild-like results are also confirmed in this paper. As shown in Figs. 1(j) and 1(k),  $-C = \sqrt{3/2}$  at the  $x = r = 0$  singularity. Along the singularity curve,  $-C$  also crosses the line of  $C = 0$  and is expected to asymptote to zero eventually as  $x$  goes to infinity. When  $C = 0$ , the energy-momentum tensor of the scalar field is zero, and the spacetime is vacuum.

(ii) Near the singularity, the Minser-Sharp mass is [25]

$$m \approx \frac{1}{8}(1 - J^2)A^{3+2C^2}e^{2\sigma_0}r^{-2C^2}. \quad (31)$$

Then the metric component  $g_{rr}$  is

$$\begin{aligned} g_{rr} &= (g^{\mu\nu}r_{,\mu}r_{,\nu})^{-1} \\ &= \left(1 - \frac{2m}{r}\right)^{-1} \\ &\approx -\frac{r}{2m} \\ &\approx -\frac{4r^{1+2C^2}}{(1 - J^2)A^{3+2C^2}e^{2\sigma_0}}. \end{aligned} \quad (32)$$

In the Schwarzschild limit,  $g_{rr} \approx -r/(2m_0)$ . The radius of the apparent horizon,  $r = 2m_{\text{BH}}$ , plotted in Fig. 1(c) shows that, for large  $x$  where  $|C|$  approaches zero, there is

$$m_0 \approx \frac{1}{8}(1 - J^2)A^3e^{2\sigma_0}. \quad (33)$$

This confirms that the spacetime near the singularity for large  $x$  asymptotes to the Schwarzschild limit. So the no-hair theorem is also valid inside black holes. This is consistent with the conclusions in Refs. [17, 19, 20].

(iii) It is interesting to see that with Eq. (33) and the first line of Eq. (16), the second line of Eq. (16) can be obtained.

(iv) We compute the proper time in (27),

$$\tau = \int_0^r (-f)^{\frac{1}{2}} dr = \frac{1}{\gamma + 4} \sqrt{\frac{\gamma + 2}{2m_0}} r^{\frac{\gamma}{2} + 2}. \quad (34)$$

Then combining Eqs. (23), (27), (29), (30) and (34), one extracts

$$p_1 = \frac{\gamma}{\gamma + 4}, \quad p_2 = p_3 = \frac{2}{\gamma + 4}, \quad q = \frac{\sqrt{8(\gamma + 1)}}{\gamma + 4}. \quad (35)$$

These parameters satisfy  $p_1 + p_2 + p_3 = 1$  and  $p_1^2 + p_2^2 + p_3^2 = 1 - q^2$ . So the solution of (28)-(30) is a Kasner solution.

## VI. SUMMARY

The dynamics near the central singularity in spherical scalar collapse toward Schwarzschild black hole formation was studied. The equations of motion behave differently in the early and late stages of the singularity curve. Approximate analytic expressions for the metric and scalar field were obtained. Some parameters for the metric functions and scalar field along the singularity curve show certain universal features. In the late stage of collapse, the spacetime near the central singularity asymptotes to the Schwarzschild limit, verifying the no-hair theorem inside black holes.

We are aware that we currently have no complete, intuitive interpretations on the result of  $\eta_{,tt} \approx \eta_{,xx} \approx \text{Constant}$  in the early stage of the singularity curve. Besides, it also may be meaningful to analytically investigate the universal features for the metric functions and scalar field along the singularity curve.

## Acknowledgments

The author is grateful to Xinliang An, Yun-Kau Lau, Junbin Li, Daoyan Wang, Xiaoning Wu and Lin Zhang for helpful discussions. This work is supported by Shandong Province Natural Science Foundation under grant No.ZR2019MA068.

## Appendix: Derivatives near the singularity curve for Schwarzschild black holes

For a Schwarzschild black hole in the Kruskal coordinates,

$$ds^2 = \frac{32m^3}{r} e^{-r/2m} (-dt^2 + dx^2) + r^2 d\Omega^2, \quad (\text{A.1})$$

the expression for  $r$  can be expressed as

$$\frac{r}{2m} = 1 + W(z), \quad (\text{A.2})$$

where

$$z = \frac{x^2 - t^2}{e}, \quad (\text{A.3})$$

and  $W$  is the Lambert  $W$  function defined by [32]

$$Y = W(Y)e^{W(Y)}. \quad (\text{A.4})$$

$Y$  can be a negative or a complex number. On the hypersurface of  $r = \text{Constant}$ ,  $z = (x^2 - t^2)/e = \text{Constant}$ . Then, in the 2D space of  $(t, x)$ , the slope  $J$  for the curve  $r = \text{Constant}$  can be expressed as

$$J \equiv \frac{dt}{dx} = \frac{x}{t}. \quad (\text{A.5})$$

From Eq. (A.4), one obtains

$$\frac{dW}{dz} = \frac{W}{z(1+W)}, \quad \text{for } z \neq \left\{0, -\frac{1}{e}\right\}, \quad (\text{A.6})$$

$$\frac{d^2W}{dz^2} = -\frac{W^2(2+W)}{z^2(1+W)^3}, \quad \text{for } z \neq \left\{0, -\frac{1}{e}\right\}. \quad (\text{A.7})$$

Then, with Eqs. (A.2), (A.6) and (A.7), one obtains

$$\frac{r_{,x}}{2m} = \frac{dW}{dz} \cdot \frac{2x}{e}, \quad (\text{A.8})$$

$$\frac{r_{,xx}}{2m} = \frac{d^2W}{dz^2} \left(\frac{2x}{e}\right)^2 + \frac{dW}{dz} \cdot \frac{2}{e}. \quad (\text{A.9})$$

Near the singularity curve,  $z = (x^2 - t^2)/e$  approaches  $-1/e$ , and  $W$  asymptotes to  $-1$ . Then Eq. (A.9) can be approximated as below,

$$\frac{r_{,xx}}{2m} \approx -\frac{4x^2}{(1+W)^3} \approx \frac{d^2W}{dz^2} \left(\frac{2x}{e}\right)^2. \quad (\text{A.10})$$

Similarly, the first- and second-order derivatives of  $r$  with respect to  $t$  can be written as

$$\frac{r_{,t}}{2m} = -\frac{W}{z(1+W)} \cdot \frac{2t}{e}, \quad (\text{A.11})$$

$$\frac{r_{,tt}}{2m} \approx -\frac{4t^2}{(1+W)^3} \approx \frac{d^2W}{dz^2} \left(\frac{2t}{e}\right)^2. \quad (\text{A.12})$$

With Eqs. (A.8) and (A.10)-(A.12), one obtains

$$\frac{r_{,x}}{r_{,t}} = -\frac{x}{t} = -J, \quad \frac{r_{,xx}}{r_{,tt}} \approx \left(\frac{x}{t}\right)^2 = J^2. \quad (\text{A.13})$$

Using  $\eta = r^2$  and Eq. (A.13), there is obviously

$$\frac{\eta_{,x}}{\eta_{,t}} = \frac{r_{,x}}{r_{,t}} = -J. \quad (\text{A.14})$$

Combining Eqs. (A.2) and (A.6)-(A.9), we arrive at

$$\frac{\eta_{,xx}}{8m^2} = \frac{rr_{,xx} + r_{,x}^2}{4m^2} = -\frac{8mW^2}{e^2z^2} \frac{x^2}{r} + \frac{2W}{ez}. \quad (\text{A.15})$$

Similarly, we obtain

$$\frac{\eta_{,tt}}{8m^2} = \frac{rr_{,tt} + r_{,t}^2}{4m^2} = -\frac{8mW^2}{e^2z^2} \frac{t^2}{r} - \frac{2W}{ez}. \quad (\text{A.16})$$

Then, near the singularity curve, there are

$$\frac{\eta_{,xx}}{8m^2} \approx -8m \frac{x^2}{r}, \quad \frac{\eta_{,tt}}{8m^2} \approx -8m \frac{t^2}{r} \quad (\text{A.17})$$

$$\frac{\eta_{,xx}}{\eta_{,tt}} \approx \left(\frac{x}{t}\right)^2 = J^2. \quad (\text{A.18})$$



Combining Eqs. (A.2)-(A.4), (A.15) and (A.16), we have

$$\frac{-rr_{,tt} - r_{,t}^2 + rr_{,xx} + r_{,x}^2}{4m^2} = \frac{8mW}{ezr} = \frac{8m}{r}e^{-r/2m}. \quad (\text{A.19})$$

So as expected, with Eq. (2), there is

$$e^{-2\sigma} = \frac{32m^3}{r}e^{-r/2m}. \quad (\text{A.20})$$

- 
- [1] J. A. Wheeler, *Geometrodynamics* (Academic Press, New York, U.S., 1962).
  - [2] M. A. Scheel and K. S. Thorne, “*Geometrodynamics: the nonlinear dynamics of curved spacetime*,” *Phys. Usp.* **57**, 342 (2014) [*Usp. Fiz. Nauk* **184**, 367 (2014)]. [[arXiv:1706.09078 \[gr-qc\]](#)]
  - [3] J. R. Oppenheimer and H. Snyder, “*On Continued Gravitational Contraction*,” *Phys. Rev.* **56**, 455 (1939).
  - [4] R. Penrose, “*Gravitational Collapse and Space-Time Singularities*,” *Phys. Rev. Lett.* **14**, 57 (1965).
  - [5] R. Price, “*Nonspherical perturbations of relativistic gravitational collapse. I. Scalar and gravitational perturbations*,” *Phys. Rev. D* **5**, 2419 (1972).
  - [6] E. Poisson and W. Israel, “*Inner-horizon instability and mass inflation in black holes*,” *Phys. Rev. Lett.* **63**, 1663 (1989).
  - [7] E. Poisson and W. Israel, “*Internal structure of black holes*,” *Phys. Rev. D* **41**, 1796 (1990).
  - [8] M. W. Choptuik, L. Lehner and F. Pretorius, “*Probing Strong Field Gravity Through Numerical Simulations*,” in *General Relativity and Gravitation: A Centennial Perspective*, edited by A. Ashtekar, B. Berger, J. Isenberg and M. A. H. MacCallum (Cambridge University Press, Cambridge, U.K., 2015), p.361-411. [[arXiv:1502.06853 \[gr-qc\]](#)]
  - [9] M. Dafermos, “*Black holes without spacelike singularities*,” *Commun. Math. Phys.* **332**, 729 (2014). [[arXiv:1201.1797 \[gr-qc\]](#)]
  - [10] M. Dafermos and J. Luk, “*The interior of dynamical vacuum black holes I: The  $C^0$ -stability of the Kerr Cauchy horizon*,” [arXiv:1710.01722 \[gr-qc\]](#).
  - [11] B. P. Abbott *et al.*, “*Observation of Gravitational Waves from a Binary Black Hole Merger*,” *Phys. Rev. Lett.* **116**, 061102 (2016). [[arXiv:1602.03840 \[gr-qc\]](#)]
  - [12] K. Akiyama *et al.* [Event Horizon Telescope Collaboration], “*First M87 Event Horizon Telescope Results. I. The Shadow of the Supermassive Black Hole*,” *Astrophys. J.* **875**, L1 (2019). [[arXiv:1602.03840 \[astro-ph.GA\]](#)]
  - [13] S. W. Hawking and G. F. R. Ellis, *The Large Scale Structure of Space-Time* (Cambridge University Press, Cambridge, UK, 1973).
  - [14] P. S. Joshi, *Gravitational Collapse and Spacetime Singularities* (Cambridge University Press, Cambridge, UK, 2007).
  - [15] D. Christodoulou, *The formation of black holes and singularities in spherically symmetric gravitational collapse* (European Mathematical Society Publishing House, Zurich, Switzerland, 2009). [[arXiv:0805.3880 \[gr-qc\]](#)]
  - [16] V. Belinski and M. Henneaux, *The Cosmological Singularity* (Cambridge University Press, Cambridge, UK, 2018).
  - [17] A. G. Doroshkevich and I. D. Novikov, “*Space-time and physical fields inside a black hole*,” *Zh. Eksp. Teor. Fiz.* **74**, 3 (1978). [*Sov. Phys. JETP* **47**, 1 (1978)]
  - [18] G. Fournodavlos and J. Sbierski, “*Generic blow-up results for the wave equation in the interior of a Schwarzschild black hole*,” *Arch. Ration. Mech. Anal.* **235**, 927 (2020). [[arXiv:1804.01941 \[gr-qc\]](#)]
  - [19] L. M. Burko, “*Homogeneous spacelike singularities inside spherical black holes*,” *Annals Israel Phys. Soc.* **13**, 212 (1997). [[arXiv:gr-qc/9711012](#)]
  - [20] L. M. Burko, “*The singularity in supercritical collapse of a spherical scalar field*,” *Phys. Rev. D* **58**, 084013 (1998). [[arXiv:gr-qc/9803059](#)]
  - [21] D. Christodoulou, “*The formation of black holes and singularities in spherically symmetric gravitational collapse*,” *Commun. Pure Appl. Math.* **44**, 339 (1991).
  - [22] X. An and R. Zhang, “*Polynomial Blow-up Upper Bounds for the Einstein-scalar field System Under Spherical Symmetry*,” *Commun. Math. Phys.* **376**, 1671 (2020). [[arXiv:2003.13330 \[math.AP\]](#)]
  - [23] X. An and D. Gajic, “*Curvature blow-up rates in spherically symmetric gravitational collapse to a Schwarzschild black hole*,” [arXiv:2004.11831 \[math.AP\]](#)
  - [24] J.-Q. Guo, D. Wang and A. V. Frolov, “*Spherical collapse in  $f(R)$  gravity and the Belinskii-Khalatnikov-Lifshitz conjecture*,” *Phys. Rev. D* **90**, 024017 (2014). [[arXiv:1312.4625 \[gr-qc\]](#)]
  - [25] J. Q. Guo, P. S. Joshi and J. T. Galvez Gherzi, “*Mass inflation and curvature divergence near the central singularity in spherical collapse*,” *Phys. Rev. D* **92**, 104044 (2015). [[arXiv:1508.02852 \[gr-qc\]](#)]
  - [26] A. V. Frolov, “*Is It Really Naked? On Cosmic Censorship in String Theory*,” *Phys. Rev. D* **70**, 104023 (2004). [[arXiv:hep-th/0409117](#)]
  - [27] P. Csiszmadia and I. Racz, “*Gravitational collapse and topology change in spherically symmetric dynamical systems*,” *Class. Quantum Grav.* **27**, 015001 (2010). [[arXiv:0911.2373 \[gr-qc\]](#)]
  - [28] J.-Q. Guo and H. Zhang, “*Dynamics in critical collapse*,” *Eur. Phys. J. C* **79**, 625 (2019). [[arXiv:1808.09826 \[gr-qc\]](#)]
  - [29] D. Garfinkle, “*Choptuik scaling in null coordinates*,” *Phys. Rev. D* **51**, 5558 (1995). [[arXiv:gr-qc/9412008](#)]
  - [30] T. W. Baumgarte and S. L. Shapiro, *Numerical Relativity* (Cambridge University Press, Cambridge, UK, 2010).
  - [31] J. Hansen, A. Khokhlov and I. Novikov, “*Physics of the interior of a spherical, charged black hole with a scalar field*,” *Phys. Rev. D* **71**, 064013 (2005). [[arXiv:gr-qc/0501015](#)]
  - [32] R. M. Corless, G. H. Gonnet, D. E. G. Hare, D. J. Jeffrey and D. E. Knuth, “*On the Lambert W function*,” *Adv. Comput. Math.* **5**, 329 (1996).